Bull Volcanol
DOI 10.1007/s00445-012-0662-5

RESEARCH ARTICLE

Cone morphologies associated with shallow marine eruptions: east Pico Island, Azores

Neil C. Mitchell · Rachelle Stretch · Clive Oppenheimer · Daniel Kay · Christoph Beier

Received: 12 June 2012 / Accepted: 15 September 2012

Abstract Eruptions in shallow water typically produce cones of volcaniclastic material. In order to identify any systematic effects of water depth and other environmental parameters on cone morphology, we have measured the heights and widths of cones in multibeam echo-sounder data from a submarine ridge extending southeast from Pico Island, Azores. XRF analyses of dredged samples show that lavas here vary compositionally from alkali basalt to trachybasalt and trachyandesite. Cones in deeper water are generally steep-sided with upper flanks close to 30°, the dip of talus at the angle of repose. However, height/width ratios of cones vary more in shallow water (200–400-m summit depth) with extreme values below 0.1; while some shallow-water cones are steep-sided as in deep water, others are much flatter. Three such cones lie on a bench at 300-m depth immediately east of Pico Island and have flank slopes of only 10–20°. We speculate that exceptionally shallow cone slopes here were produced by forced spreading of the erupting columns on reaching the water–air density barrier.

Keywords Cone morphologies · Shallow marine eruptions · Pico Island · Volcaniclastic material

Editorial responsibility: P-S Ross

N. C. Mitchell (✉) · D. Kay
School of Earth, Atmospheric and Planetary Sciences,
University of Manchester,
Williamson Building, Oxford Road,
Manchester M13 9PL, UK
e-mail: neil.mitchell@manchester.ac.uk

R. Stretch · C. Oppenheimer
Department of Geography, University of Cambridge,
Downing Place,
Cambridge CB2 3EN, UK

C. Beier
GeoZentrum Nordbayern, University of Erlangen-Nürnberg,
Schlossgarten 5,
91054 Erlangen, Germany

Introduction

Eruptions in shallow water typically produce volcaniclastic cones, which are common around volcanic islands. They are thought to arise from explosive eruptions and through interaction of lava flows with ambient water (White et al. 2003), with pyroclasts depositing on outward-facing slopes of the cones at the angle of repose of the material. Until recently, there have been few observations of the in situ process of cone formation, except for sightings of pumice and other particles floating on the ocean surface (Siebe et al. 1995; Kaneko et al. 2005). Processes have generally been inferred from the analysis of the particles deposited from the erupting vents (Kokelaar and Durant 1983; Cashman and Fiske 1991; Yamamoto et al. 1991; Fiske et al. 1998; Fiske et al. 2001) or recovered from the water surface (Siebe et al. 1995). Over the last decade, researchers have begun making more direct observations (Mitchell 2012), such as at Rota-1 volcano in the west Pacific erupting at 550-m depth (Embley et al. 2006), where the ambient pressure reduces the danger to instruments from explosions. Chadwick et al. (2008a) described video observations, taken using a remotely operated vehicle, of mildly explosive activity and reported measurements of acoustic noise, which included 2–6-min explosive bursts. Surficial landslides on the flanks of the cone have been recorded using the acoustic measurements and repeat surveying of the bathymetry (Chadwick et al. 2012). Similar repeat surveying has been carried out on Monowai submarine volcano in the Kermadec arc, revealing periods of construction and sector collapses. These have acted to rework deposits from around the summit of the cone and re-deposit them on its lower flanks (Chadwick et al. 2008b). Watts et al. (2012) surveyed this cone with multibeam sonar immediately before and after an eruption in 2011, which was recorded separately in hydrophone (T wave) data. Combining the multibeam and T wave datasets, they were able to show that the eruption rate was similar to that inferred for subaerial edifices on other

Published online: 27 September 2012

volcanic ocean islands (Crisp 1984). In contrast to these relatively explosive eruptions, Gaspar et al. (2003) reported a more effusive eruption at 300–1,000 m on a ridge to the west of Terceira Island in the Azores in which expanding gas produced 'balloons' of basaltic lava. As has been observed elsewhere (Siebe et al. 1995), these 'balloons' remained on the surface before sinking in the Terceira case after a 15-min delay.

There have been no close-range observations of large submarine eruption columns in shallow water as far as we are aware. During explosive eruptions into water, the eruption column is expected to lose considerable momentum due to the surrounding fluid being more dense and viscous than air (Cashman and Fiske 1991; White et al. 2003). However, the density difference between particles and seawater is much smaller than between particles and air. Equivalently sized particles can therefore be uplifted in water columns of smaller upward velocity than in atmospheric plumes. Gas retained in vesicles provides further buoyancy, which is later lost when water vapour or steam condenses on cooling. If the erupting column comes into contact with the sea surface, it is expected to halt and spread on encountering that density contrast, forming a thin eruption umbrella (provided that the water depth is not so shallow that the momentum in the column can allow it to breach the sea surface, as occurred during the formation of Surtsey Island (Moore 1985)). During the spreading phase, particles within the umbrella may be transported by currents (Cashman and Fiske 1991).

Around Hawai'i, exceptionally flat cones with height to width (H/W) ratios of 0.1–0.2 are common, with some H/W ratios approaching 0.04 (Clague et al. 2000; Mitchell et al. 2002; Smith et al. 2002; Umino et al. 2006). Unlike the cones described herein, these flat cones have been interpreted to have formed from lava extrusions in the form of lava lakes (Clague et al. 2000; Zhu et al. 2002). The low sulphur contents of lava samples recovered from these cones compared with their source composition suggest that they arise where the magma has already degassed before erupting on the seabed, for example, during eruption in subaerial lava lakes (Clague et al. 2000). Thus, the route by which magma is transported towards the final eruption location (whether or not opportunities for degassing exist before eruption) could be an important factor over whether pointy (volcaniclastic) or flat (effusive) cones form.

Evidence of vigorous pyroclastic eruptions in deep water has been reported, e.g., at 4,200-m depth near the Hawaiian Islands, which Clague and coworkers (Clague et al. 2002; Davis and Clague 2006) have suggested may involve high volatile contents. Based on samples collected along the Mid-Atlantic Ridge running through the Azores islands, Bonatti (1990) argued that the magmas forming the Azores originate from melting of mantle rich in H_2O and other volatiles rather than anomalously high mantle temperatures, a theme more recently corroborated by modelling (Asimow et al. 2004) and p–T estimates from major elements of lavas from the islands (Beier et al. 2012). A volatile-rich source and limited prior degassing such as that evident for Hawai'i may explain the prevalent pointy cones that we will describe later.

The submarine ridge extending southeast from the eastern ridge of Pico Island (Fig. 1) is the result of volcanism in a transtensional plate-tectonic regime (Searle 1980; Lourenço et al. 1998). According to Madeira and Brum da Silveira (2003), the subaerial volcanic products on the east of Pico Island (Madalena V. Complex) comprise lavas and scoria cones. They are probably of Holocene age based on their pristine textures and radiocarbon dates and since the unit includes three historical eruptions identified elsewhere on the island. Nunes (1999) dated a flow almost at the easterly extremity of the island from associated organic material as 2000 y BP using ^{14}C. Delicate morphologies of submarine lavas in near-shore areas were recorded in the same multibeam sonar dataset that we present here (Mitchell et al. 2008), originating from subaerial lavas that entered the sea. These are unlikely to have survived surf erosion during rising sea level, providing further support for a Holocene age. An exception is a lava flow adjacent to the extreme east of the island, which appears to have been abraded, leaving an unusually smooth surface.

The lavas forming the island are alkali basalts with minor hawaiites (França et al. 2006; Beier et al. 2012). Further samples from the eastern subaerial ridge of the island were reported previously (Mitchell et al. 2008). They reveal a common liquid line of descent, similar to other Azorean islands (Beier et al. 2006; Beier et al. 2008), though a number of samples were less evolved. Compared with the rest of Pico Island, the subaerial ridge lavas are slightly more evolved on average and more diverse. Broadly speaking, those data confirmed the alkali basalt composition of the primary magma, though with varying degrees of olivine and clinopyroxene fractionation. During two cruises of the R/V *Poseidon* (232 and 286), rock dredges were taken from the ridge (along the white lines with annotation "POS", etc., in Fig. 1).

The present study concerns an analysis of shapes of cones in multibeam echo-sounder data collected in 2003 (Mitchell et al. 2008) along with deeply towed ("TOBI") sidescan sonar data collected in 1999 (Ligi et al. 1999; Stretch et al. 2006). The results reveal that simple pointy cones occur at all depths but some cones are flatter (smaller height/width ratio) in shallower water. We unfortunately lack seismic data capable of resolving the internal structures of these features, so there is some ambiguity in interpreting individual cone shapes. Besides a suite of dredge samples, we also lack in situ information, in particular representative grain-size data. Nevertheless, the trends in the dataset

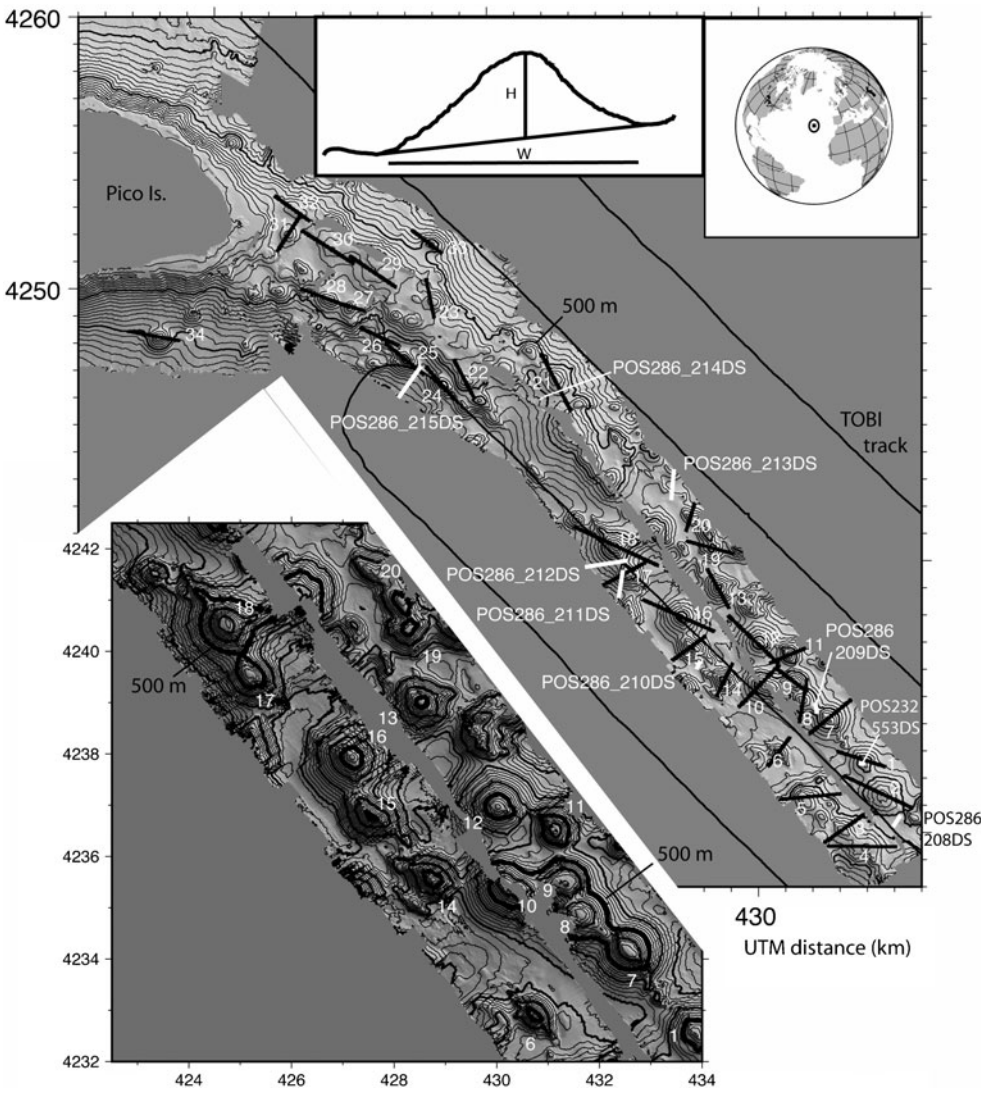

Fig. 1 Multibeam echo-sounder dataset from the submarine ridge extending south-east of Pico Island. *Bold black lines numbered with white lettering* show where topographic cross-sections of cones were taken. Also shown are the sites of rock dredges (*bold white lines* annotated POS, etc.) and the path of the TOBI deep-tow vehicle used in surveying the ridge in 1999 (Stretch et al. 2006) (*solid line*). Bathymetry data have been gridded at 25 m and contoured at 50 m (500-m intervals are shown in *bold*). Coordinates are Universal Transverse Mercator projection (zone 26) distances in kilometers, which provide scale. *Top-right inset* locates the study area. *Top-centre* inset shows a typical cone measurement of height (*H*) and width (*W*) (cone 2). *Lower-left inset* shows an enlargement of the bathymetry (10-m grid) contoured at 20 m, with 100- and 500-m contours in *medium bold* and *heavy bold*, respectively

overall appear consistent with volcaniclastic deposits produced from shallow marine eruptions. We interpret the flatter cones to arise from spreading of the erupting column caused by the abrupt air–sea density interface.

Data collection and analysis

The data collection on the University of Azores R/V Arquipelago and data processing are described in Mitchell et al. (2008). The data were collected with a portable multibeam echo-sounder temporarily mounted on the vessel. A small movement of the sonar transducers relative to the vessel (and hence relative to installed vessel motion sensors) during strong vessel movements led to some across-track rippling of the data (higher wave conditions were experienced immediately east of Pico Island). However, the data are sufficient to resolve cone morphology. The gridded data were loaded into the GeoMapApp software (Ryan et al. 2009) and cross-sections of the cones were extracted as marked by the bold dark lines in Fig. 1. Maps and bed gradient calculations were created with GMT software (Wessel and Smith 1991). Where cones are elongated, cross-sections were made perpendicular to the cone's long axis, but other orientations were in some cases necessary, for instance, to ensure that the base of the cones could be interpreted from their profiles (hence, the gradients of some of the flank profiles are biased towards smaller values).

The cross-sections are plotted centred on the summit locations horizontally in Fig. 2 and both horizontally and vertically in Fig. 3. Cone height and width were interpreted from the 32 cones identified in Fig. 1 by fitting a line to the inflection points on either side of each cone profile to account for the substrate gradient as illustrated in the top-centre inset of Fig. 1. Unfortunately, the cone bases are not everywhere easily identified because a gradient changes gradually and the topography can be confused by the rugged pre-existing relief of the ridge; hence, individual measurements have an uncertainty of

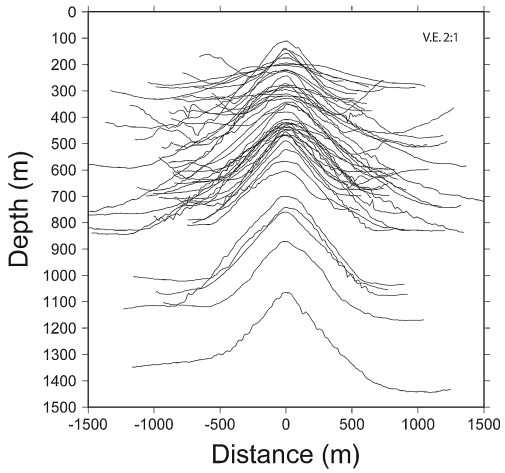

Fig. 2 Bathymetry profiles of the submarine cones centred laterally according to their summit locations. Vertical exaggeration is 2:1

up to ±5–10 %. Therefore, trends in this dataset are interpreted rather than individual values. A further 16 submarine cones surveyed around Pico, Faial and São Jorge (central Azores islands) outside the area shown in Fig. 1 were also interpreted and included in this analysis to increase the size of the dataset. On the basis of surficial morphology and dimensions, these further cones appear no different from the Pico submarine ridge cones studied here. These combined morphometric parameters are plotted in Fig. 4a, b and listed in Table 1. Also shown in Fig. 4a are parameters of subaerial scoria cones from the eastern ridge of Pico Island, measured in the same way from the Shuttle Radar Topography Mission data (Ryan et al. 2009). As scoria cones may be more familiar to readers, these are included to give a sense of scale.

Figure 5 shows a gradient map and enlarged bathymetry of the area immediately east of Pico Island. Figure 6 shows the acoustic backscattering data collected with the multibeam sonar data for the area marked in the inset to Fig. 5 (high backscattering is shown with a dark tone). This image suffers from artefacts (Mitchell 1991) along the trackline (marked "Art" in Fig. 6) caused by the flat seabed assumption used by the mosaicking software; nevertheless, some features and their acoustic textures can be observed as marked. Cone numbering follows that in Fig. 5.

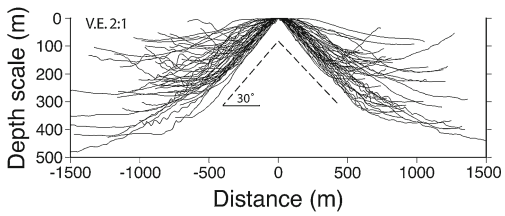

Fig. 3 Bathymetry profiles of the submarine cones centred on their summit locations. For comparison, *dashed lines* represent the dip of a perfect cone with 30° flanks. Vertical exaggeration is 2:1

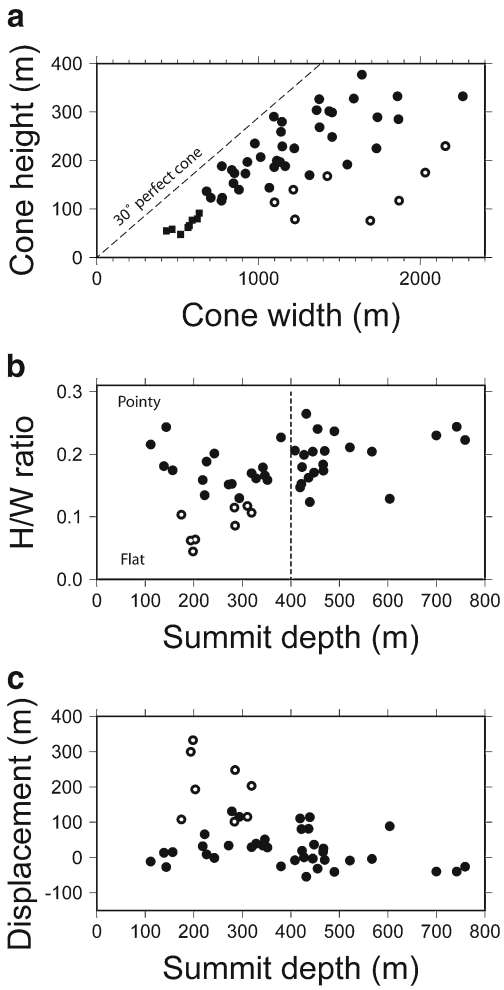

Fig. 4 Cone morphometric parameters. **a** Width versus height for the subaerial (*squares*) and submarine (*circles*) cones. For comparison, *dashed line* shows the trend expected for a perfect cone with 30° slopes. **b** *H*/*W* ratio versus summit depth for the submarine cones. *Vertical dashed line* at 400-m depth marks an arbitrarily chosen boundary between deep and shallow populations. **c** The mean particle displacement (in excess of that expected for an equivalent-volume steep cone) implied by the cone *H* and *W* values (see text for calculation). In **a** to **c**, the *open circles* represent the flatter cones defined by $H/W < 0.12$

Seabed backscatter data over the Pico Ridge were also collected with a sidescan sonar on the TOBI deeply towed vehicle in 1999 (Ligi et al. 1999; Stretch et al. 2006; Stretch 2007). In Figs. 7 and 8, these data are displayed with high backscatter in white and low backscatter in dark grey. During interpretation, the backscatter data can be viewed along with the bathymetry so that the interpreter can allow for any effect of seabed relief in modulating the acoustic angle of incidence (Mitchell and Somers 1989), but image variations are typically caused by seabed type variations rather than relief. Superimposed are a selection of thin-section images (Fig. 7) and mineralogy (Fig. 8) of samples collected by dredging on the R/V *Poseidon* during cruises 232 and 286 (also located in Fig. 1). Bulk compositions of some of these

Table 1 Dimensions (heights *H* and basal widths *W*) of submarine cones measured here. Cones 1–32 are shown in Fig. 1; cones 33–48 were measured from other parts of this multibeam sonar dataset (not shown)

Cone identifier	*H* (m)	*W* (m)	Summit depth (m)
1	192	1,549	439
2	230	2,156	319
3	140	1,216	284
4	175	2,033	285
5	225	1,729	294
6	235	979	455
7	333	1,859	342
8	189	1,166	329
9	187	1,099	319
10	289	1,737	346
11	259	1,140	380
12	285	1,867	422
13	299	1,457	471
14	290	1,097	432
15	327	1,377	490
16	394	2,423	437
17	328	1,590	409
18	467	3,050	279
19	197	1,133	467
20	197	932	522
21	168	1,425	311
22	123	776	352
23	144	1,069	223
24	225	1,222	467
25	249	1,455	448
26	174	853	446
27	117	773	272
28	174	919	227
29	76	1,692	199
30	117	1,870	194
31	114	1,100	175
32	79	1,227	203
33	200	1,113	423
34	280	1,147	742
35	378	1,640	700
36	207	1,013	567
37	189	773	143
38	154	847	138
39	304	1,360	760
40	333	2,265	420
41	230	114	427
42	140	879	219
43	180	836	111
44	123	706	157
45	137	679	243
46	170	1,315	604
47	269	1,379	870
48	302	1,439	1,065

samples measured by XRF in the University of Kiel are shown in Table 2 (for details, see Beier et al. (2006, 2008)).

Observations

Physiography of the ridge

The multibeam sonar data cover only the summit and upper flanks of the submarine ridge, including the region of high acoustic backscattering visible in Fig. 7. Based on the 30-kHz frequency of the TOBI sonar, a maximum penetration of order 1 m can be expected depending on the angle of incidence and sediment attenuation properties (Mitchell 1993), so this area comprises bare rock, talus or thinly sedimented seafloor.

The ridge is superimposed with cones of varied sizes and aspect ratios. Where elongated, their major axes are generally oriented parallel to the overall ridge trend. The lower-left inset to Fig. 1 illustrates the typical morphology of the deeper cones. The regular spacing of contours on the flanks of these cones suggests relatively uniform gradients. Small ridges running parallel to the overall trend of the survey tracks can be observed emanating from some cones, such as cones 18 and 7. Although many of these lie parallel to the vessel track such that an acoustic artefact cannot be ruled out, we suspect that they represent ridges produced by volcanic effusion above the same erupting dykes that formed the cones. Minor indentations of contours on the cone flanks running oblique to the artefacts mentioned earlier suggest surficial landsliding or sector collapses (e.g., cones 16 and 12). The flatter summit regions are generally narrow, up to only a few hundred metres at most.

Dark blue in the gradient map highlights areas of gentler (<5°) gradients. This includes the abrasion shelf immediately east of Pico Island and farther east beyond that an area where the ridge has a somewhat flat summit bench with superimposed cones. The bathymetry corresponding to this area is also shown enlarged in the lower-left inset to Fig. 5.

Dredged rock samples

Analysis of thin sections of the samples, which are generally porphyritic, revealed the presence of pyroxene, olivine and plagioclase in varying degrees of alteration. Hyaloclastites were identified at various depths from 325 to 780 m. (We use the term “hyaloclastite” here in the general sense of volcaniclastic rock containing glassy fragments (Thorpe and Brown 1985; Batiza et al. 1984).) High loss-on-ignition (LOI) values in the XRF analyses show that most samples are significantly altered. The three analyses in Table 2 (from sites marked in Fig. 8) have the smallest LOI. A high proportion of dredges also recovered carbonates

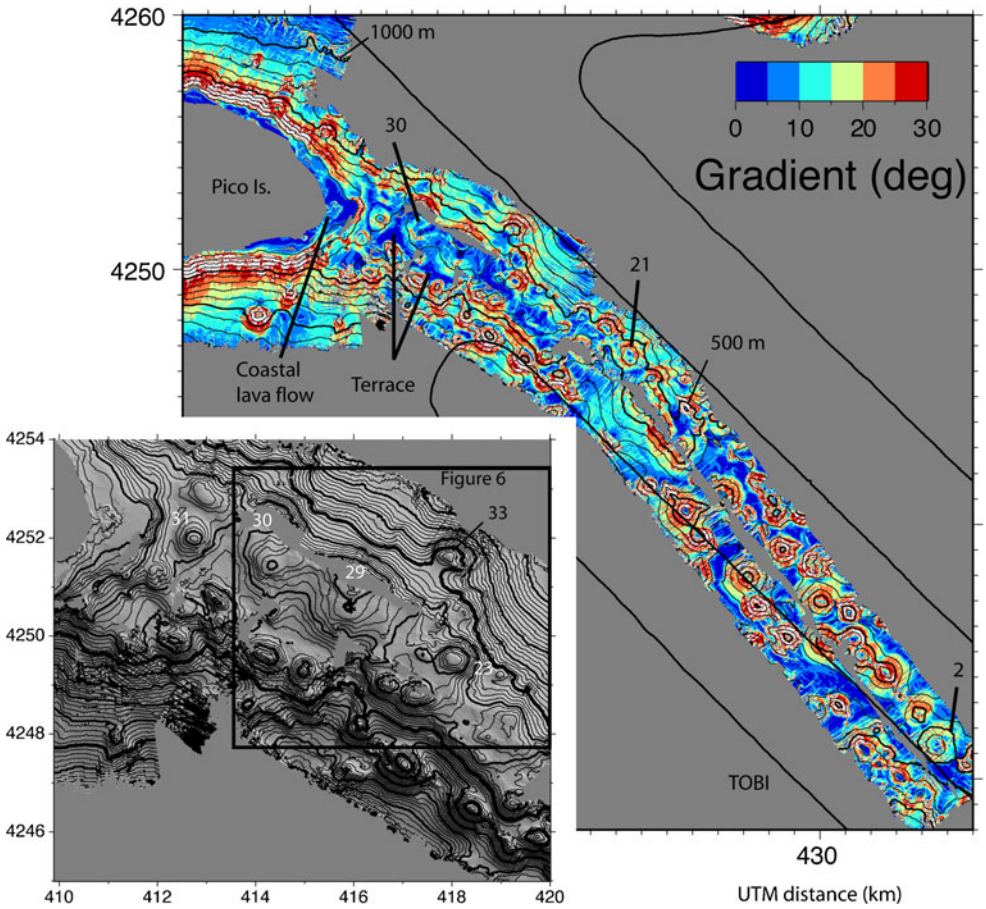

Fig. 5 Gradient map of the submarine ridge extending southeast of Pico Island as derived from 25-m gridded multibeam data. *Continuous lines* marked *TOBI* show the path of the TOBI deep-towed vehicle for cross-referencing with Fig. 7. Bathymetry contours are shown at every 100 m with the 500-m contour in *bold*. *Lower-left inset* shows an enlargement of the bench immediately east of the island (contours at every 20 m with 100 and 500 m in *bold* and *heavy bold*, respectively) derived from 10-m gridded multibeam data. The *rectangle* locates the acoustic backscattering data shown in Fig. 6. Coordinates are Universal Transverse Mercator projection distances in kilometers (zone 26), which provide scale

and corals. Therefore, much of the ridge has probably not been resurfaced by lavas recently. However, one sample of fresh lava was recovered in the north of the area (Fig. 8). The northernmost sample within the multibeam survey area was classified as alkali basalt (215DS), whereas the other two dredges yielded more evolved trachybasalts and trachyandesites. No particular correlation was found between bulk compositions and seabed texture in the TOBI sidescan sonar data (Stretch 2007).

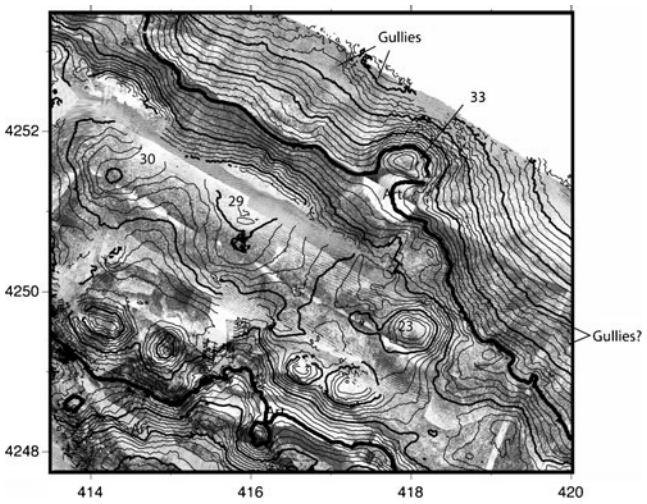

Fig. 6 Acoustic backscattering mosaic derived from the multibeam sonar data (high backscattering shown with *dark tone*). *Cone numbers* correspond with those in Fig. 5 *inset*, which includes the bounds of the map. Note the smooth texture under cones 29 and 30

As the vesicularity of lavas may affect their viscosities (Wallace and Anderson 2000) and reflect magma volatile content, Stretch (2007) measured the vesicularity of the R/V *Poseidon* dredge samples (Fig. 7) in thin sections, as well as the dry bulk density (a proxy for porosity) using the water replacement method. The results are shown in Fig. 9. Bold lines represent either analyses of single dredge hauls or averages where more than one sample in a dredge haul were analysed. Although there are problems of sample size with the former method, and effects of alteration and fracture porosity in the latter, any strong variation with depth was expected still to be apparent in the results, but none is observable. The sample vesicularity and density data also showed no relationship to surface texture in the TOBI sonar images (Stretch 2007).

Cone geometrical characteristics

In Figs. 2 and 3, the flanks of the cones appear to have relatively consistent gradients, though tending to be concave upwards towards the cone bases. This curvature could partly

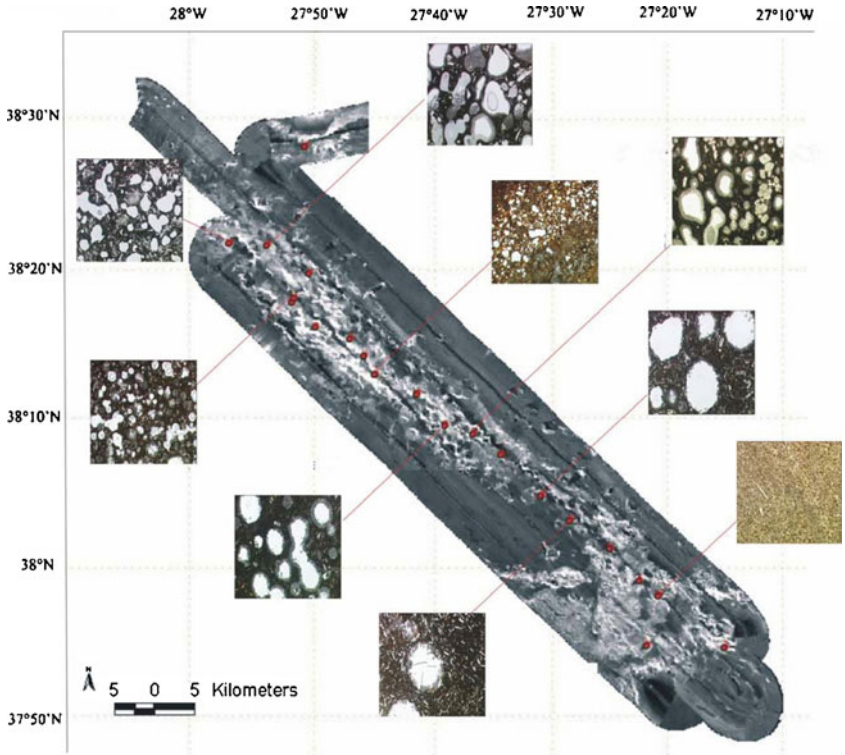

Fig. 7 Thin-section images of dredge samples collected on R/V *Poseidon* cruises 232 and 286. The b*ackground* is a greyscale map of TOBI deep-tow sidescan sonar data (Stretch et al. 2006). *White* represents high backscatter. The thin-section images are about 5 mm across

arise from the runout of debris on the slopes as described for subaerial scree slopes (Young 1972; Selby 1993) or perhaps an effect of shaking by occasional earthquakes as suggested for the submarine slopes of Hawai'i (Lee et al. 1994). The cone summits generally lack either broad plateaux or pits observed in other submarine cones (Chadwick et al. 2008a, b). In Fig. 4a, cone basal widths (W) and heights (H) of both subaerial (square symbols) and submarine (circles) cones are shown together on a scatter plot. A general increase in height with increasing width is apparent. With the subaerial cones excluded, however, the data show less central tendency or correlation. Everywhere the cone gradients are less than 30° (a gradient delimiting the angle of repose of submarine basaltic talus of 28–30° measured from acoustic transponder-navigated submersible dive transects (Mitchell et al. 2000)); the data in Fig. 4a fall to the right of the dashed line representing simple 30° cones.

Smith and coworkers (Smith 1988, 1996) have idealised seamounts as truncated cones in order to study variations in cone shape. Although some cones in Fig. 3 lack a flatter summit region, most have a small rounded or flatter summit, presumably representing the finite area of the vent and material deposited around it. If the cone summit width is W_0, the height H and basal width W for a perfect truncated cone are related by $H=0.5(W-W_0)\tan\theta$, where θ is the average dip angle of the flanks. Because there are few data in Fig. 4a and their measurement is somewhat subjective, obtaining θ and W_0 by regression is not worthwhile here. We instead note that the main body of data (solid symbols in Fig. 4a lying in the upper-left of the dataset) could be modelled with flank gradients of 30° and with W_0 equal to about 200 m or more. Because of the upward curvature of the flank profiles, this W_0 value effectively represents the wider basal area of low gradients below 30° as well as the summit.

In Fig. 4b, the ratio H/W ("steepness") is plotted against summit depth. Whereas the maximum H/W is high across the full range of depths (pointy cones occur in both deep and shallow water), the range of H/W values generally declines with increasing summit depth. In the shallower water, there are more cones with flatter profiles. Cones with $H/W<0.12$ are highlighted with unfilled circle symbols in Fig. 4a–c. Statistical tests on such small sample sizes are relatively unreliable, but a simple calculation of mean and standard error of the data separated at an arbitrarily chosen 400-m depth suggests that the trends are just significant. The mean and standard errors of H/W are 0.148±0.024 and 0.196±0.024 (2σ) for the 0–400- and >400-m summit depths, respectively.

Detailed morphology of the Pico Ridge summit bench

The gradients in Fig. 5 reflect the trends inferred from Fig. 4b. Cone flanks typically have gradients of 25–30° (red areas in the figure). However, on the summit bench of the ridge near the island, the cone flanks are generally shallower (<20°). The lower-left inset to Fig. 5 shows an enlargement of the bathymetry there with 20-m contours.

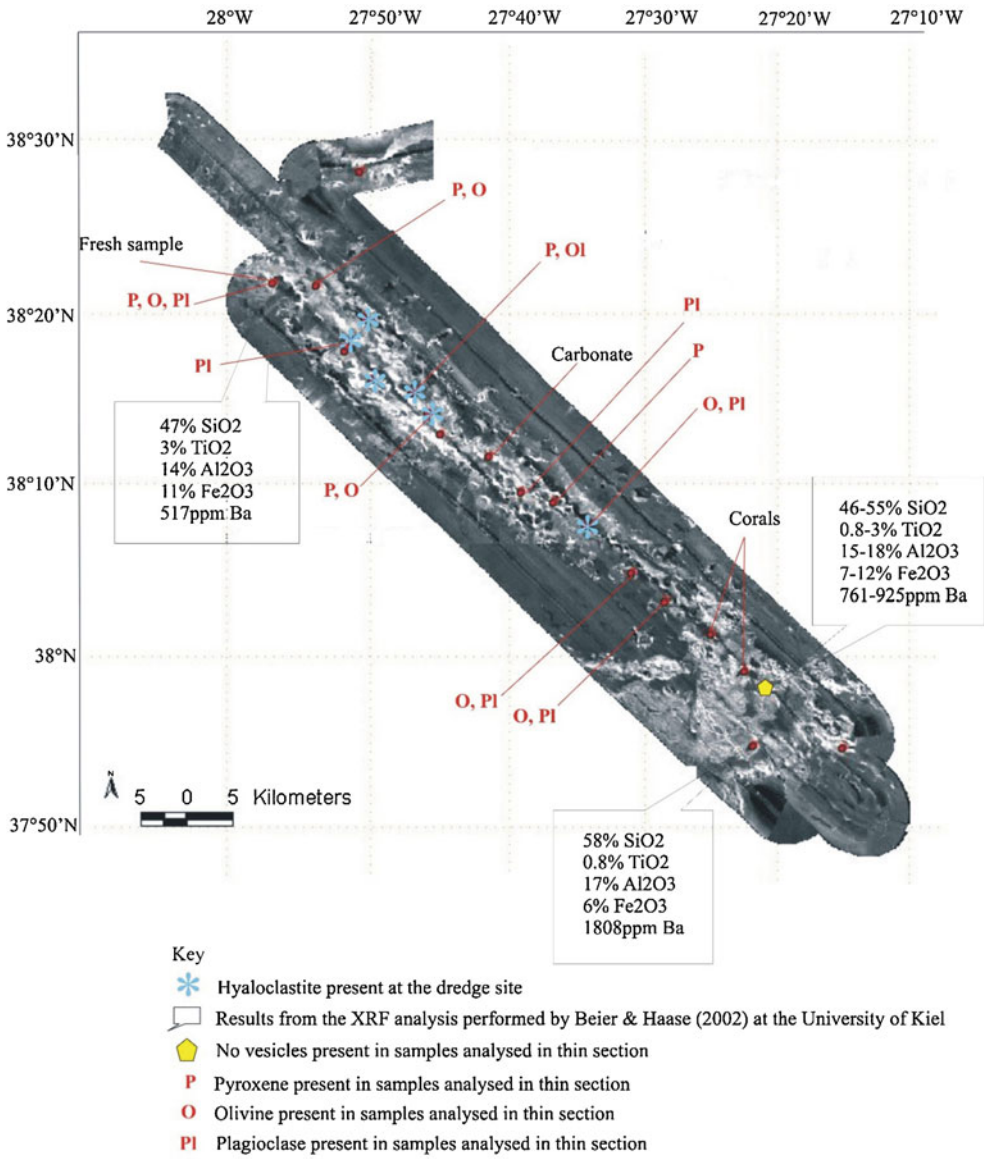

Fig. 8 Mineral and hyaloclastite presence in the R/V *Poseidon* dredge samples

Four cones (23, 29, 30 and 31) have notably more widely spaced contours than cones down the flanks of the ridge. Two summit cones are visible with relatively steep flanks (cones 23, 31 and one not numbered immediately south of 31 and southwest of 30), so not all summit cones are anomalously flat in the shallower waters.

Acoustic backscattering data

In the absence of high-resolution seismic data and samples over this area, we appeal to the acoustic backscattering data to provide clues to surface sediment or rock presence and morphology (Blondel and Murton 1997). The reader should ignore dominant SW–SE trends in these data (Fig. 6), which are caused by the ship tracks and joins between adjacent swaths. Between them, the region over cones 29 and 30 is relatively acoustically smooth and featureless, aside from speckle expected of monochromatic imagery (Mitchell 1995). This texture is as expected for a sediment-covered, relatively smooth seabed and we interpret it here as probably representing a mound of volcaniclastic particles. In contrast, the summit bench of the ridge between cones 23 and 29 has a mottled texture, suggestive of lava flow exposures. This mottled texture arises from the contrasts between bare rock and sediment and from acoustic shadowing by rugged terrain, being described previously as hummocky or bulbous in deeply towed sidescan sonar images of lava (Smith et al. 1995). Also visible are bands of high backscattering extending down the flanks of the ridge coinciding with linear depressions in the bathymetry. These represent gullies produced by sediment gravity flows. This suggests that there has been some erosion though apparently not so extensively to affect the cone statistics we will discuss in the following section.

Table 2 Compositions of a selection of R/V *Poseidon* cruise 286 dredged samples taken from sites marked in Fig. 1. Oxides are given in weight percent

Sample	196 DS2	198 DS5	215 DS1
Max depth (m)	1,139	1,100	844
SiO_2	58.13	47.95	46.89
TiO_2	0.81	3.11	2.94
Al_2O_3	17.38	15.51	14.26
$Fe_2O_3{}^T$	6.04	11.04	11.09
MnO	0.14	0.19	0.16
MgO	2.05	3.85	8.21
CaO	4.05	8.32	10.27
Na_2O	4.16	3.83	3.21
K_2O	4.61	2.03	1.19
P_2O_5	0.33	0.77	0.52
LOI	1.1	2.22	0.07
Total	98.8	98.82	98.81
Ba (ppm)	1,808	761	517
Cr (ppm)	b.d.l.	4	317
Ni (ppm)	b.d.l.	b.d.l.	143
Zn (ppm)	67	124	103
Rb (ppm)	83	54	30
Sr (ppm)	597	619	574
Zr (ppm)	148	297	264
Classification	Trachyandesite	Trachybasalt	Alkali basalt

Measurements were made by X-ray fluorescence in the Institut für Geowissenschaften, Universität Kiel (Beier et al. 2006; Beier et al. 2008)

LOI loss on ignition, *b.d.l.* below detection limit

Discussion

The generally consistent cone flank gradients (Figs. 2 and 3) are interpreted as formed by volcaniclastic particles supplied from vents at the central summits of the cones and with particles depositing near the angle of repose. In Fig. 4a, however, some cones lie below a simple trend expected of cone flanks enlarging at the 28–30° angle of repose (Mitchell et al. 2000). Some of these flatter cones lie in the shallower water on the summit bench (Fig. 5, inset). The lack of surface and internal samples of these cones and the lack of seismic reflection images of them unfortunately limit the reliability of our interpretation of these features. Flowing lava is indeed possible in shallow water without immediate disaggregation because flow structures are imaged around the coasts of Pico (Mitchell et al. 2008), so effusive origins for these cones are not entirely ruled out. Nevertheless, the following evidence suggests that these cones were likely also produced by explosive eruptions.

The presence of sediment (which we suggest is volcaniclastic) covering the cones implied by the backscatter data is supported by the finer texture of the bathymetry data (Fig. 5), which show smooth, rounded cone morphologies. Given the apparent exposure or only thin sediment cover on the lavas farther down the ridge suggested by high backscatter in the TOBI data (Fig. 7), it seems unlikely that the flat cones are covered in mud to obscure hummocky textures in the more shallow regions where currents are stronger. The flat cones described by Clague et al. (2000) were found to be deeper than 500 m and had flat tops with sharp breaks of slope to steep flanks (i.e. coin-like shapes); in contrast, the flat cones described here all occur in shallow water (none in deep water) and have more rounded profiles. Smith and Cann (1999) interpreted some submarine cones as rootless, having been emplaced by eruption over lava tubes. Thus, a magma that has degassed on land, such as within lava lakes, might conceivably feed an effusive eruption in shallow water via tubes. However, it is difficult to envision lava tubes feeding cones 2, 29 and 30 from land as down-gradient paths lie away from the summit of the ridge to the north and south (Fig. 5). Overall, the simplest interpretation of the flatter cones is that they are formed of granular material much like the 30° pointy cones and differ only because of processes associated with eruption into shallow water.

The potential for surface waves to have influenced the shallow cones

Some of these cones may have erupted before or during the Last Glacial Maximum (LGM), so possible influences of surface waves should be considered in flattening the tops of cones. During the LGM, sea level probably dropped to 135 m below the present level based on a eustatic lowstand

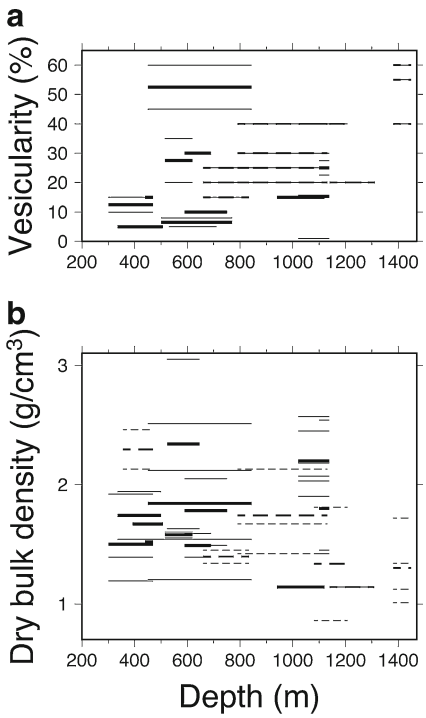

Fig. 9 Estimates of **a** vesicularity and **b** bulk density of samples collected on R/V *Poseidon* (Stretch 2007). Vesicularity was estimated in thin section and density measurements were made using the water displacement method. *Horizontal bars* represent the depth extent at which the dredges were in contact with the bed. *Continuous lines* represent densities of samples from the Pico submarine ridge (dredge sites marked in Fig. 7) and *dashed lines* from ridges adjacent to Faial and São Jorge islands. *Bold lines* represent averages of data (*fine lines*) from single dredge hauls or where only one sample from a haul was analysed

estimate from northern Australia (Yokoyama et al. 2000) and as the Azores are a long way from the ice sheet loads (i.e. glacio-isostatic movements are small). Modelling predicts a subsidence rate of ~1-1.5 mm year^{-1} here from glacio-isostasy (Argus and Peltier 2010). We also discount rapid subsidence of the island as there is little evidence of the kinds of erosional benches seen around Hawai'i (Moore 1987) except examples to the southwest of Topo volcano farther west, where they lie only down to 90-m depth (Mitchell et al. 2008; Fig. SM15 of the "Electronic supplementary material"), still above the LGM level. The shelf break around Pico Island also does not appear unusually deep. Wave erosion depth in these materials can be conservatively judged from the depth to which Surtla (near Surtsey, Iceland) was eroded because the wave climate in south of Iceland is stronger than in the Azores (estimated 100-year return value of significant wave height is >24 m compared with ~15 m in the Azores (Sterl and Caires 2005)). According to Kokelaar and Durant (1983), the summit of volcaniclastic materials on Surtla was eroded down to 45-m depth over 18 years following its eruption. Thus, surfaces from 135 to 180 m below modern sea level were potentially affected by wave erosion during the LGM if created before the LGM. Any cone summits now below 180 m should have been unaffected by wave erosion in the absence of glacio-isostatic movements or below 200 m if the 1–1.5 mm year^{-1} glacio-isostatic adjustment (Argus and Peltier 2010) was extrapolated over the past 20 kyr. In Fig. 4b, four cones lie within this 200-m limit. Nevertheless, the assumptions behind this calculation are extreme and four further cones at around 300-m depth also have H/W of ~0.1. These cone profiles are rounded and lack a flat surface typical of a wave-eroded rock platform (Sunamura 1992). At least some of these low H/W values therefore arose from other mechanisms.

Flat cones formed during shallow explosive eruptions

Following Cashman and Fiske (1991), we interpret anomalous H/W as caused by the forced spreading of columns during explosive eruptions by the air–water density barrier and further displacements of particles by tidal and other currents during their fallout to the seabed. The amount of spreading can be estimated from geometry. If a perfect cone is formed from particles depositing after displacement from a central point, the mean horizontal displacement of those particles can be shown by integration to equal $W/4$ or, alternatively, $H/2\tan(\theta)$. Therefore, the tendency for H/W to become smaller with some values <0.1 towards shallower water represents an increased displacement for those cones with the smallest H/W values. This implies additional lateral displacement by currents and other processes. For each measured cone, we estimated the equivalent width W_0 expected for a cone of the same volume (idealised with $V=\pi W^2 H/12$) but with a more typical pointy cone H/W ratio of 0.2. This was then used to estimate the anomaly $(W-W_0)/2$ or implied mean additional displacement of particles. The results shown in Fig. 4c are likely to be noisy but nevertheless imply lateral displacements of >100 m for all the flatter cones.

Figure 10 shows the geometry of cone 29 (2:1 vertical exaggeration). From the cone dimensions (H= 76 m, W_0=1,692 m), the mean additional displacement is 333 m, which is illustrated by the arrows in Fig. 10. Also shown are the depth of sea level at the LGM and maximum depth of wave influence at that time, assuming the Surtla erosion depth (dashed and dotted lines, respectively). Although sea level has fluctuated, it has stood at around 50 m below present day for much of the Quaternary (Miller et al. 2005). Therefore, the eruption is most likely to have involved a subaqueous buoyant column 150 m in height (present summit depth to around 50 m depressed sea level), so the ratio of the extra lateral displacement to water depth is probably 2:1.

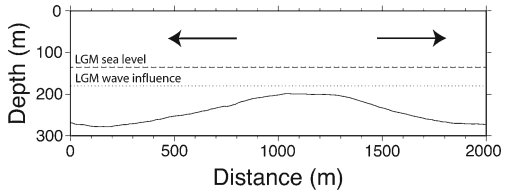

Fig. 10 The topographic profile of cone 29 (2:1 vertical exaggeration) shown along with the predicted depths of sea level and maximum wave influence during the Last Glacial Maximum. Also shown (*solid arrows*) are the mean additional displacements of particles required to produce this flat cone compared with a cone of the same volume but with *H*/*W* a more typical 0.2. Flattening is interpreted here as due to spreading of the eruption column on encountering the air–water density interface and influence of currents on falling particles (Cashman and Fiske 1991)

Translation of particles by water currents

Evaluating viability of advection of pyroclasts by currents is difficult here as there are few current data available. Bashmachnikov (2006) describes data from current meters installed for 3–4 months within the channels between Faial and Pico and between Pico and São Jorge Islands nearby. Spring tidal currents in the former reached 32 cms^{-1} and were relatively uniform over the water column aside from a bottom friction layer. In contrast, the meter installed in the Pico–São Jorge channel recorded currents smaller by approximately a factor of three (M_2 tides). Currents have also been modelled numerically by Juliano (2010), taking account tidal and wind forcing. Her results for the 0–50-m depth interval suggest a kinetic energy flux of 25 $kWhm^{-2}$ around the eastern end of Pico island where the shallow volcanic cones lie, about a factor of two less than the 50 $kWhm^{-2}$ maximum flux within the Faial–Pico channel, which is high there because of a funnelling effect between the islands. As the kinetic energy in a streaming current is proportional to the square of the current, the currents off east Pico should be around $32/\sqrt{2}$ or a modest 23 cms^{-1}.

In order for a particle to be translated laterally by >100 m falling from the eruption column umbrella at the surface, we assume that it falls ~250 m (Fig. 10) through a uniform current of 23 cms^{-1}, implying a terminal velocity of <60 cm/s. According to Fig. 2 of Cashman and Fiske (1991), a particle of dry bulk density 2.5 gcm^{-3} would have a terminal velocity <60 cms^{-1} if it has a diameter of <1 cm and greater diameters for densities <2.5 g/cm^3 (densities from Fig. 9b). In practice, particles are likely to fall in groups rather than individually (Cashman and Fiske 1991) as also seen in experiments of comparable falling suspensions (Parsons et al. 2001). Grains of a given diameter are likely to fall faster than expected from calculations of simple isolated spheres, so 1 cm is a maximum. This simple calculation also ignores grain shape effects.

Although we have no vibracore samples that would properly constrain the cone grain size distributions, where the dredge hauls recovered carbonate-cemented material, particles of this size and less were present. On the basis of these calculations, we therefore concur with Cashman and Fiske (1991) that currents probably can influence the final depositional geometry of the finer submarine erupted particles. However, the aspect ratios of the flatter cones in the bathymetry contours in Fig. 5 inset are not noticeably different from those of the pointy cones. Tidal currents would be expected to displace particles to NE and SW, leading to more elliptical contours. Thus, tidal spreading seems to be minor in practice. This may imply that particle size is generally greater than 1 cm or other processes such as time of eruption limited tidal spreading.

Variability of cone shapes in shallow water

The variability in *H*/*W* ratio in the shallower depths (presence of both flat and pointy cones) could arise from a variety of factors. These include eruption timing in relation to the spring tide, particle sizes and porosities (which will reflect magma rheology and fragmentation and hence magma composition, volatile abundance, degassing history, crystallinity, etc.; Table 2) and sea level at the time of eruption. If observations of shallow water eruptions are planned, we suggest that column and umbrella dynamics could be addressed further by monitoring eruptions down to 400-m depth, with additional geophysical studies of cone geometry combined with sampling of deposits.

Conclusions

Cones of the Pico submarine ridge have a more varied height/width ratio in 200–400-m depths ($0.045<H/W<0.24$) than in deeper water ($H/W>0.12$). Whereas the shallower cones vary from flat to pointy, the deeper cones are all pointy. We interpret this as implying that wider dispersion of particles away from the vent occurs in the shallower water sites where 'headroom' above the cone is less than 400 m. Following Cashman and Fiske (1991), we suggest that an enforced spreading of the erupting column by the abrupt density change at the water–air interface explains the flatter cones. However, although fallout calculations of the kind suggested by Cashman and Fiske (1991) based on the known tidal currents in the Azores suggest that spreading of particles by the currents should be important for particle sizes <1 cm, the cone shapes are not obviously elongated. This mechanism therefore appears not to have been important in shaping the cones here.

Acknowledgments We thank the officers and crews involved in collecting the data on R/Vs *Arquipelago* (2003), *Urania* (1999) and *Poseidon* (cruises 232 and 286) and Chief Scientists Colin Devey and

Karsten M. Haase. We thank especially Marco Ligi (ISMAR-Bologna, Italy) for organising the cruise on *Urania* as well as other CNR scientists involved in the data processing (mosaicking) and the Southampton TOBI group for running the sonar. Thanks are also due to the marine biologists of the University of the Azores for their help in running the *Arquipelago* cruise (Fernando Tempera and Eduardo Isidro). Fernando Tempera and Rui Quartau kindly located the current meter data for us. ChB acknowledges inspiration in Peter's café with excellent views of Pico. Reviews by Young Kwan Sohn, John Smellie and associate editor Pierre-Simon Ross were very helpful in revising this manuscript. Funding was provided by a variety of agencies including the EASSS and CNR (TOBI survey) and the Royal Society, British Council, HEFCW, the Regional Directorate for Science and Technology of the Azores and Portuguese projects MAR-INOVA and MAROV (multibeam survey).

References

Argus DF, Peltier WR (2010) Constraining models of postglacial rebound using space geodesy: a detailed assessment of model ICE-5G (VM2) and its relatives. Geophys J Int 181:697–723

Asimow PD, Dixon JE, Langmuir CH (2004) A hydrous melting and fractionation model for mid-ocean ridge basalts: application to the Mid-Atlantic Ridge near the Azores. Geochem Geophys Geosys. doi:10.1029/2003GC000568

Bashmachnikov I (2006) Upper layer water structure and dynamics in the region of Triangle (Faial, Pico, S. Jorge) from the CTD and moorings data, obtained during the R/V "Arquipelago" cruises. University of the Azores, 11 pp.

Batiza R, Fornari DJ, Vanko DA, Lonsdale P (1984) Craters, calderas, and hyaloclastites on young Pacific seamounts. J Geophys Res 89:8371–8390

Beier C, Haase KM, Hansteen TH (2006) Magma evolution of the Sete Cidades volcano, São Miguel, Azores. J Petrol 47:1375–1411

Beier C, Haase KM, Abouchami W, Krienitz M-S, Hauff F (2008) Magma genesis by rifting of oceanic lithosphere above anomalous mantle: Terceira Rift, Azores. Geochem Geophys Geosyst 9: Paper Q12013

Beier C, Haase KM, Turner SP (2012) Conditions of melting beneath the Azores. Lithos 144–145:1–11

Blondel P, Murton BJ (1997) Interpretation of sidescan sonar imagery. Wiley, Chichester, p 317

Bonatti E (1990) Not so hot "hot spots" in the oceanic mantle. Science 250:107–111

Cashman KV, Fiske RS (1991) Fallout of pyroclastic debris from submarine volcanic eruptions. Science 253:275–280

Chadwick WW, Cashman KV, Embley RW, Matsumoto H, Dziak RP, de Ronde CEJ, Lau TK, Deardorff ND, Merle SG (2008a) Direct video and hydrophone observations of submarine explosive eruptions at NW Rota-1 volcano, Mariana arc. J Geophys Res. doi:10.1029/2007JB005215

Chadwick WW, Wright IC, Schwartz-Schampera U, Hyvernaud O, Reymond D, de Ronde CEJ (2008b) Cyclic eruptions and sector collapses at Monowai submarine volcano, Kermadec arc: 1998–2007. Geochem Cosmochim Acta. doi:10010.11029/12008GC002113

Chadwick WW, Dziak RP, Haxel JH, Embley RW, Matsumoto H (2012) Submarine landslide triggered by volcanic eruption recorded by in situ hydrophone. Geology 40:51–54

Clague DA, Moore JG, Reynolds JR (2000) Formation of flat-topped volcanic cones in Hawai'i. Bull Volcanol 62:214–233

Clague DA, Uto K, Satake K, Davis AS (2002) Eruption style and flow emplacement in the submarine North Arch Volcanic Field, Hawaii. In: Takahashi E, Lipman PW, Garcia MJ, Naka J, Aramaki S (eds) Hawaiian volcanoes, deep underwater perspectives. Am Geophys Union Geophys Monogr 128, Washington, DC, pp 65-84

Crisp JA (1984) Rates of magma emplacement and volcanic output. J Volcanol Geotherm Res 20:177–211

Davis AS, Clague DA (2006) Volcaniclastic deposits from the North Arch volcanic field, Hawaii: explosive fragmentation of alkalic lava at abyssal depths. Bull Volcanol 68:294–307

Embley RW, Chadwick WW, Baker ET, Butterfield DA, Resing JA, de Ronde CEJ, Tunnicliffe V, Lupton JE, Juniper SK, Rubin KH, Stern RJ, Lebon GT, Nakamura K, Merle SG, Hein JR, Wiens DA, Tamura Y (2006) Long-term eruptive activity at a submarine arc volcano. Nature 441:494-497

Fiske RS, Cashman KV, Shibata A, Watanabe K (1998) Tephra dispersal from Myojinsho, Japan, during its shallow submarine eruption of 1952–1953. Bull Volcanol 59:262–272

Fiske RS, Naka J, Iizasa K, Yuasa M, Klaus A (2001) Submarine silicic caldera at the front of the Izu-Bonin arc, Japan: voluminous seafloor eruptions of rhyolite pumice. Geol Soc Am Bull 113:813–824

França Z, Tassinari CCG, Cruz JV, Aparicio AY, Araña V, Rodrigues BN (2006) Petrology, geochemistry and Sr–Nd–Pb isotopes of the volcanic rocks from Pico Island—Azores (Portugal). J Volcanol Geotherm Res 156:71–89

Gaspar JL, Queiroz G, Pacheco JA, Ferreira T, Wallenstein N, Almeida MH, Coutinho R (2003) Basaltic lava balloons produced during the 1998–2001 Serreta Submarine Ridge eruption (Azores). In: White JDL, Smellie JL, Clague DA (eds) Subaqueous explosive volcanism. Am Geophys Union Geophysical Monogr 140, Washington, DC, pp 205-212

Juliano M (2010) Evaluation of ocean tidal/currents energy in the Azores region. In: Green Islands Azores. Ponta Delgada, Azores, 28th May 2010, http://www.green-islands-azores.uac.pt/admin/ficheiros/uploads/MIT_Tides_PontaDelgada_2010_2028_2005.pdf (accessed 31/05/2012)

Kaneko T, Yasuda A, Shimano T, Nakada S, Fujii T, Kanazawa T, Nishizawa A, Matsumoto Y (2005) Submarine flank eruption preceding caldera subsidence during the 2000 eruption of Miyakejima Volcano. Japan Bull Volcanol 67:243–253

Kokelaar BP, Durant GP (1983) The submarine eruption and erosion of Surtla (Surtsey), Iceland. J Volcanol Geotherm Res 19:239–246

Lee HJ, Torresan ME, McArthur W (1994) Stability of submerged slopes on the flanks of the Hawaiian Islands, a simplified approach. U.S. Geological Survey Open-File Report 94-638:1–54

Ligi M, Mitchell NC, Marani M, Gamberi F, Penitenti D, Carrara G, Rovere M, Portaro R, Centorami G, Bortoluzzi G, Jacobs C, Rouse I, Flewellen C, Whittle S, Terrinha P, Freire Luis J, Lourenco N (1999) Giant volcanic ridges amongst the Azores islands. EOS Trans AGU 80(Fall Meet Suppl):F913

Lourenço N, Miranda JM, Luis JF, Ribeiro A, Victor LAM, Madeira J, Needham HD (1998) Morpho-tectonic analysis of the Azores volcanic plateau from a new bathymetric compilation of the area. Mar Geophys Res 20:141–156

Madeira J, Brum da Silveira A (2003) Active tectonics and first paleoseismological results in Faial, Pico and S. Jorge islands (Azores, Portugal). Annals Geophys 46:733–761

Miller KG, Kominz MA, Browning JV, Wright JD, Mountain GS, Katz ME, Sugarman PJ, Cramer BS, Christie-Blick N, Pekar SF (2005) The Phanerozoic record of global sea-level change. Science 310:1293–1298

Mitchell NC (1991) Improving GLORIA images using sea beam data. J Geophys Res 96:337–351

Mitchell NC (1993) A model for attenuation of backscatter due to sediment accumulations and its application to determine sediment thickness with GLORIA sidescan sonar. J Geophys Res 98:22477–22493

Mitchell NC (1995) Representing backscatter fluctuations with a PDF convolution equation, and its application to study backscatter

variability in side-scan sonar images. IEEE Trans Geosci Remote Sens 33:1328–1331
Mitchell NC (2012) Hot, cracking rocks deep down. Nature Geosc 5:444–445
Mitchell NC, Somers ML (1989) Quantitative backscatter measurements with a long range side-scan sonar. IEEE J Oceanic Eng 14:368–374
Mitchell NC, Tivey MA, Gente P (2000) Slopes of mid-ocean ridge fault scarps from submersible observations. Earth Planet Sci Lett 183:543–555
Mitchell NC, Masson DG, Watts AB, Gee MJR, Urgeles R (2002) The morphology of the flanks of volcanic ocean islands: a comparative study of the Canary and Hawaiian hotspot islands. J Volcanol Geotherm Res 115:83–107
Mitchell NC, Beier C, Rosin P, Quartau R, Tempera F (2008) Submarine lava flows around the coasts of Pico Island, Azores. Geochem Geophys Geosyst. doi:10.01029/02007GC001725
Moore JG (1985) Structure and eruptive mechanisms at Surtsey Volcano, Iceland. Geol Mag 122:649–661
Moore JG (1987) Subsidence of the Hawaiian ridge. In: Decker RW, Wright TL, Stauffer PH (eds) Volcanism in Hawaii. US Geol Surv Prof Paper 1350, pp 85–100
Nunes JC (1999) A actividade vulcânica na Ilha do Pico do Plistocénico Superior ao Holocénico: Mecanismo eruptivo e hazard vulcânico. Ph.D. thesis, Departamento de Geociencias. Universidade dos Acores, Ponta Delgada, p 355
Parsons JD, Bush J, Syvitski JPM (2001) Hyperpycnal flow formation with small sediment concentrations. Sediment 48:465–478
Ryan WBF, Carbotte SM, Coplan JO, O'Hara S, Melkonian A, Arko R, Wiessel RA, Ferrini V, Goodwillie A, Nitsche F, Bonczkowski J, Zemsky R (2009) Global multi-resolution topography synthesis. Geochem Geophys Geosys. doi:10.1029/2008GC002332
Searle RC (1980) Tectonic pattern of the Azores spreading centre and triple junction. Earth Plan Sci Lett 51:415–434
Selby MJ (1993) Hillslope materials and processes. Oxford University Press, Oxford, p 451
Siebe C, Komorowski J-C, Navarro C, McHone J, Delgado H, Cortes A (1995) Submarine eruption near Socorro Island, Mexico: geochemistry and scanning electron microscopy studies of floating scoria and reticulite. J Volcanol Geotherm Res 68:239–271
Smith DK (1988) Shape analysis of Pacific seamounts. Earth Planet Sci Lett 90:457–466
Smith DK (1996) Comparison of the shapes and sizes of seafloor volcanoes on Earth and “pancake” domes on Venus. J Volcanol Geotherm Res 73:47–64
Smith DK, Cann JR (1999) Constructing the upper crust of the Mid-Atlantic Ridge: A reinterpretation based on the Puna Ridge, Kilauea Volcano. J Geophys Res 104:25379–25399
Smith DK, Cann JR, Dougherty ME, Lin J, Spencer S, Macleod C, Keeton J, McAllister E, Brooks B, Pascoe R, Robertson W (1995) Mid-Atlantic Ridge volcanism from deep-towed side-scan sonar images, 25°-29°N. J Volcanol Geotherm Res 67:233–262
Smith DK, Kong LSL, Johnson KTM, Reynolds JR (2002) Volcanic morphology of the submarine Puna Ridge, Kilauea volcano. In: Takahashi E, Lipman PW, Garcia MJ, Naka J, Aramaki S (eds) Hawaiian volcanoes, deep underwater perspectives. Am Geophys Union Geophys Monogr 128, Washington, DC, pp 125-142
Sterl A, Caires S (2005) Climatology, variability and extrema of ocean waves: the web-based KNMI/ERA-40 wave atlas. Int J Climatol 25:963–977
Stretch R (2007) A morphometric and textural analysis of the submarine volcanic ridges of the Azores Plateau. Ph.D. thesis, Faculty of Earth Sciences and Geography, University of Cambridge,Cambridge, 360 pp.
Stretch R, Mitchell NC, Portaro RA (2006) A morphometric analysis of the submarine volcanic ridge of Pico Island. J Volcanol Geotherm Res 156:35–54
Sunamura T (1992) Geomorphology of rocky coasts. Wiley, New York
Thorpe RS, Brown GC (1985) The Field description of igneous rocks. Open University Press, Milton Keynes
Umino S, Nonaka M, Kauahikaua J (2006) Emplacement of subaerial pahoehoe lava sheet flows into water: 1990 Kupaianaha flow of Kilauea volcano at Kaimu Bay, Hawai'i. Bull Volcanol 69:125–139
Wallace P, Anderson AT (2000) Volatiles in magmas. In: Sigurdsson H, Houghton B, McNutt SR, Rymer H, Stix J (eds) Encyclopedia of volcanoes. Academic, San Diego, pp 149–170
Watts AB, Peirce C, Grevemeyer I, Paulatto M, Stratford W, Bassett D, Hunter JA, Kalnins LM, de Ronde CEJ (2012) Rapid rates of growth and collapse of Monowai submarine volcano, Kermadec Arc. Nature Geosc 5:510–515
Wessel P, Smith WHF (1991) Free software helps map and display data. Eos Trans Am Geophys Union 72:441
White JDL, Smellie JL, Clague DA (2003) Introduction: a deductive outline and topical overview of subaqueous explosive volcanism. In: White JDL, Smellie JL, Clague DA (eds) Subaqueous explosive volcanism. Am Geophys Union Geophysical Monogr 140, Washington, DC, pp 1-23
Yamamoto T, Soya T, Suto S, Uto K, Takada A, Sakaguchi K, Ono K (1991) The 1989 submarine eruption off eastern Izu Peninsula, Japan: ejecta and eruption mechanisms. Bull Volcanol 43:301–308
Yokoyama Y, Lambeck K, De Deckker P, Johnston P, Fifield LK (2000) Timing of the Last Glacial Maximum from observed sea-level minima. Nature 406:713–716
Young A (1972) Slopes. Oliver and Boyd, Edinburgh, p 288
Zhu W, Smith DK, Montési LGJ (2002) Effects of regional slope on viscous flows: a preliminary study of lava terrace emplacement at submarine volcanic rift zones. J Volcanol Geotherm Res 119:145–159